MARKOV CHAIN MODELS OF COUPLED INTRACELLULAR CALCIUM CHANNELS: KRONECKER STRUCTURED REPRESENTATIONS AND BENCHMARK STATIONARY DISTRIBUTION CALCULATIONS

HILARY DEREMIGIO[†], PETER KEMPER[‡],

M. DREW LAMAR[†], and GREGORY D. SMITH[†]

[†]*Department of Applied Science,* [‡]*Department of Computer Science,*
The College of William and Mary, Williamsburg, VA 23187

Mathematical models of calcium release sites derived from Markov chain models of intracellular calcium channels exhibit collective gating reminiscent of the experimentally observed phenomenon of stochastic calcium excitability (i.e., calcium puffs and sparks). We present a Kronecker structured representation for calcium release site models and perform benchmark stationary distribution calculations using numerical iterative solution techniques that leverage this structure. In this context we find multi-level methods and certain preconditioned projection methods superior to simple Gauss-Seidel type iterations. Response measures such as the number of channels in a particular state converge more quickly using these numerical iterative methods than occupation measures calculated via Monte Carlo simulation.

1. Introduction

The stochastic gating of voltage- and ligand-gated ion channels in biological membranes that is observed by single channel recording techniques is often modeled using discrete-state continuous-time Markov chains (CTMCs).[1,2] While these single channel models can be relatively simple (e.g., two physicochemically distinct states) or complex (hundreds of states), most include only two conductance levels (closed and open). For example, a transition state diagram for a three-state calcium (Ca^{2+})-regulated channel activated by sequential binding of two Ca^{2+}ions is given by

$$
\begin{array}{ccccc}
 & k_a^+ c & & k_b^+ c & \\
C_1 & \rightleftharpoons & C_2 & \rightleftharpoons & O_1 \\
 & k_a^- & & k_b^- &
\end{array}
\tag{1}
$$

where $k_i^+ c$ and k_i^- with $i \in \{a, b\}$ are transition rates with units of reciprocal time, k_i^+ is an association rate constant with units of $\text{conc}^{-1} \text{time}^{-1}$, and c is the $[Ca^{2+}]$ near the channel. If this local $[Ca^{2+}]$ is specified, the transition-state diagram of the channel (1) defines a CTMC that takes on values in the state-space (C_1, C_2, O_1). The experimentally observable conductance of this stochastically gating channel is the aggregated process of transitions between the closed and open classes of states: $\mathcal{C} = \{C_1, C_2\}$ and $\mathcal{O} = \{O_1\}$.

The scientific literature developing stochastic models for the behavior of ion channels is largely focused on single channels or populations of independent channels. One notable exception is the work of Ball and colleagues analyzing interacting aggregated CTMC models of membrane patches containing several ion channels.[3,4] A second example, the subject of this paper, are simulations of clusters of intracellular Ca^{2+}-regulated Ca^{2+} channels—inositol 1,4,5-trisphosphate receptors (IP_3Rs) and ryanodine receptors (RyRs)—located on the surface of the endoplasmic reticulum or sarcoplasmic reticulum membrane—that give rise to localized intracellular $[Ca^{2+}]$ elevations known as Ca^{2+} puffs and sparks.[5–9]
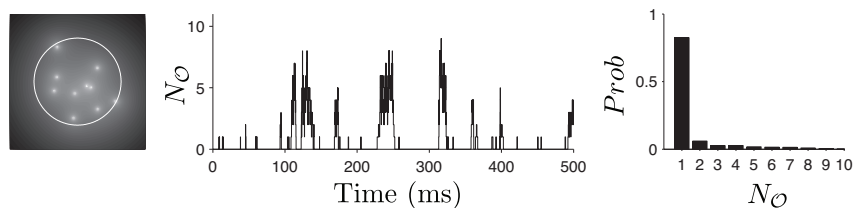

Fig. 1.   Left: Local $[Ca^{2+}]$ near 3×3 μm ER membrane with Ca^{2+} channels modeled as 0.05 pA point sources with positions randomly chosen from a uniform distribution on a disc of radius 2 μm. Buffered Ca^{2+} diffusion is modeled as in Ref. 10. Middle: Stochastic Ca^{2+} excitability reminiscent of Ca^{2+} puffs/sparks. Right: Probability distribution of the number of open channels leading to a puff/spark *Score* of 0.39.

When Markov chain models of Ca^{2+}-regulated Ca^{2+} channels such as (1) are coupled via a mathematical representation of buffered diffusion of intracellular Ca^{2+}, simulated Ca^{2+} release sites may exhibit the phenomenon of "stochastic Ca^{2+} excitability" where the IP_3Rs or RyRs open and close in a concerted fashion[10,11] (see Fig. 1 for representative simulation) . Such models are stochastic automata networks (SANs) that involve a large number of functional transitions, that is, the transition probabilities of one automata (i.e., an individual channel) may depend on the local $[Ca^{2+}]$ and thus the state of the other channels. The experimentally observable quantity is ei-

ther the local $[\text{Ca}^{2+}]$ or the number of channels in the open class of states, $N_{\mathcal{O}}(t)$ (see Fig. 1, middle).

The relationship between single channel kinetics of Ca^{2+}-regulated channels and the emergent phenomenon of Ca^{2+} puffs and sparks is not well understood. However, if each release site configuration is known, several informative response measures can be determined from the steady-state probability distribution. For example, the so-called puff/spark $Score$[10] given by $\text{Var}[f_{\mathcal{O}}]/\text{E}[f_{\mathcal{O}}]$ is the index of dispersion of the steady-state fraction of open channels, $f_{\mathcal{O}} = N_{\mathcal{O}}/N$ (see Fig. 1, right). This response measure takes values between 0 and 1, and a puff/spark $Score$ of greater than approximately 0.3 indicates the presence of Ca^{2+} excitability. However, Ca^{2+} release sites are composed of 5–250 channels and this leads to a state-space explosion that makes numerical calculation of the stationary distribution of model Ca^{2+} release sites difficult.

2. Formulation of Model

In this paper we consider two single channel models: the three-state Ca^{2+}-activated channel described above (1) and a six-state model that includes both fast Ca^{2+} activation and slow Ca^{2+} inactivation, processes that are important aspects of the dynamics of both IP_3Rs and RyRs. The six-state model assumes two identical channel subunits that both require Ca^{2+} binding to enter a permissive state and include a second Ca^{2+}-mediated transition into a long-lived non-permissive state (for transition state diagram and parameters see Ref. 12).

In both the three- and six-state models, Ca^{2+}-mediated transitions out of open states can be accelerated due to the increase in local $[\text{Ca}^{2+}]$ when a Ca^{2+}-regulated Ca^{2+} channel is open.[13,14] Assuming the formation and collapse of Ca^{2+} microdomains are fast compared to channel gating, we can denote the background and domain $[\text{Ca}^{2+}]$ experienced by the channel when closed and open as c_{∞} and c_d, respectively. With this assumption the three- and six-state single channel models take the form $Q = K_- + (c_{\infty}I + c_dI_{\mathcal{O}})K_+$ where K_- and K_+ are $M \times M$ matrices that collect the unimolecular (k_i^-) and bimolecular (k_i^+) transition rates, $I_{\mathcal{O}} = \text{diag}\{e_{\mathcal{O}}\}$, and $e_{\mathcal{O}}$ is a $M \times 1$ vector indicating open states of the single channel model.[10] In our model formulation, the interaction between channels is mediated through the buffered diffusion of intracellular Ca^{2+} (see Ref. 10 for a complete description). For the purposes of this paper we do not assume any particular cell type with known release site ultrastructure (e.g., cardiac myocytes with channels arranged in a dyad) and instead

consider that the N channels at the Ca^{2+} release site have positions chosen from a two-dimensional uniform distribution on a disc of radius 0.1–2.0 μm (i.e., constant surface density; see Fig. 1, left). When in the open state, each channel contributes to the landscape of $[Ca^{2+}]$ throughout the Ca^{2+} release site and influences the local $[Ca^{2+}]$ experienced by other channels. For simplicity we assume that the formation and collapse of individual peaks within the Ca^{2+} microdomain occur quickly compared to channel gating. We also assume the presence of a single high concentration Ca^{2+} buffer and the validity of superposing local $[Ca^{2+}]$ increases due to each of the N channels.[15,16] Thus, channel interactions can be summarized by an $N \times N$ 'coupling matrix' $C = (c_{ij})$ that gives the increase over c_∞ experienced by channel j when channel i is open.

2.1. *Instantaneous Coupling of Two* Ca^{2+}*-Regulated* Ca^{2+} *Channels*

In the case of two identical Ca^{2+}-regulated Ca^{2+} channels the interaction matrix takes the form

$$C = \begin{pmatrix} c_d & c_{12} \\ c_{21} & c_d \end{pmatrix}$$

and the expanded generator matrix is given by $Q^{(2)} = Q_-^{(2)} + Q_+^{(2)}$ where

$$Q_-^{(2)} = K_- \otimes I + I \otimes K_- \qquad (2)$$

collects the unimolecular transition rates and $\otimes$ denotes the Kronecker product (see Ch. 9 in Ref. 17). The transition rates involving Ca^{2+} take the form

$$Q_+^{(2)} = D_1^{(2)} \left(K_+ \otimes I \right) + D_2^{(2)} \left(I \otimes K_+ \right), \qquad (3)$$

where the two terms represent Ca^{2+}-mediated transitions of each channel. The diagonal matrices $D_1^{(2)}$ and $D_2^{(2)}$ give the $[Ca^{2+}]$ experienced by channel 1 and 2, respectively, in every configuration of the release site, that is,

$$D_1^{(2)} = \text{diag} \left\{ c_\infty \left(e \otimes e \right) + c_d \left(e_\mathcal{O} \otimes e \right) + c_{21} \left(e \otimes e_\mathcal{O} \right) \right\}$$
$$= c_\infty \left(I \otimes I \right) + c_d \left(I_\mathcal{O} \otimes I \right) + c_{21} \left(I \otimes I_\mathcal{O} \right)$$

and similarly for $D_2^{(2)}$. Using the Kronecker identities such as $\left(I \otimes I_\mathcal{O} \right) \left(I \otimes K_+ \right) = I \otimes I_\mathcal{O} K_+$, Eq. 3 can be rearranged as

$$Q_+^{(2)} = c_\infty K_+^{(2)} + c_d \left(I_\mathcal{O} K_+ \otimes I \right) + c_{12} \left(I_\mathcal{O} \otimes K_+ \right)$$
$$+ c_{21} \left(K_+ \otimes I_\mathcal{O} \right) + c_d \left(I \otimes I_\mathcal{O} K_+ \right) \qquad (4)$$

where $K_+^{(2)} = K_+ \otimes I + I \otimes K_+$. Combining Eqs. 2 and 4 and simplifying, $Q^{(2)}$ can be written compactly as

$$Q^{(2)} = A_d \otimes I + I_{\mathcal{O}} \otimes A_{12} + A_{21} \otimes I_{\mathcal{O}} + I \otimes A_d \tag{5}$$

where $A_d = K_- + c_\infty K_+ + c_d I_{\mathcal{O}} K_+$, and $A_{ij} = c_{ij} K_+$.

2.2. *Instantaneous Coupling of N* $\mathbf{Ca^{2+}}$*-Regulated* $\mathbf{Ca^{2+}}$ *Channels*

In the case of N channels coupled at the Ca^{2+} release site, the expanded generator matrix—i.e., the SAN descriptor—is given by

$$Q^{(N)} = Q_-^{(N)} + Q_+^{(N)} \tag{6}$$

$$Q_-^{(N)} = \bigoplus_{n=1}^N K_- = \sum_{n=1}^N I^{(n-1)} \otimes K_- \otimes I^{(N-n)} \tag{7}$$

$$Q_+^{(N)} = c_\infty K_+^{(N)} + \sum_{i,j=1}^N c_{ij} \left(Y_{ij}^1 Z_{ij}^1 \otimes \cdots \otimes Y_{ij}^N Z_{ij}^N \right) \tag{8}$$

$$Y_{ij}^n = \begin{cases} I_{\mathcal{O}} & \text{for } i = n \\ I & \text{otherwise} \end{cases} \qquad Z_{ij}^n = \begin{cases} K_+ & \text{for } j = n \\ I & \text{otherwise} \end{cases} \tag{9}$$

where $I^{(n)}$ is an identity matrix of size M^n and $K_+^{(N)} = \oplus_{n=1}^N K_+$. Combining Eqs. 7 and 8 and simplifying, $Q^{(N)}$ can be written as

$$Q^{(N)} = \sum_{i,j=1}^N X_{ij}^1 \otimes \cdots \otimes X_{ij}^N \tag{10}$$

$$X_{ii}^n = \begin{cases} A_d & \text{for } i = n \\ I & \text{otherwise.} \end{cases} \qquad \text{and} \qquad X_{ij}^n = \begin{cases} I_{\mathcal{O}} & \text{for } i = n \\ A_{ij} & \text{for } j = n \\ I & \text{otherwise} \end{cases} \quad \text{for } i \neq j$$

where $A_d = K_- + c_\infty K_+ + c_d I_{\mathcal{O}} K_+$, and $A_{ij} = c_{ij} K_+$. Note that all states of the expanded Markov chain $Q^{(N)}$ are reachable, the matrices I, $I_{\mathcal{O}}$, A_d, A_{ij}, and X_{ij}^n are all $M \times M$, and $2N^2 - N$ of the N^3 matrices denoted by X_{ij}^n are *not* identity matrices.

3. Stationary Distribution Calculations

The limiting probability distribution of a finite irreducible CTMC is the unique stationary distribution $\boldsymbol{\pi}^{(N)}$ satisfying global balance,[17] that is,

$$\boldsymbol{\pi}^{(N)} Q^{(N)} = \mathbf{0} \quad \text{subject to} \quad \boldsymbol{\pi}^{(N)} \boldsymbol{e}^{(N)} = 1 \tag{11}$$

where $Q^{(N)}$ is the Ca^{2+} release site SAN descriptor (Eq. 10) and $\boldsymbol{e}^{(N)}$ is an $M^N \times 1$ column vector of ones. Although Monte Carlo simulation techniques such as Gillespie's Method[18] can be implemented to estimate response measures such as the puff/spark *Score*, this is an inefficient approach when the convergence of the occupation measures to the limiting probability distribution is slow. This problem is compounded by the state-space explosion that occurs when the number of channels (N) or number of states per channel (M) is large (i.e., physiologically realistic). Both space requirements and quality of results can be addressed using the Kronecker representation (Eq. 10) and various iterative numerical methods to solve for $\boldsymbol{\pi}^{(N)}$.

Many methods are available to solve Eq. 11 with different ranges of applicability (see Ref. 17 for review). For larger models, a variety of iterative methods are applicable including the method of Jacobi, and Gauss-Seidel, along with variants that use relaxation, e.g., Gauss-Seidel with relaxation (`SOR`). Such methods require space for iteration vectors and $Q^{(N)}$ but usually converge quickly. More sophisticated projection methods—e.g., the generalized minimum residual method (`GMRES`) and the method of Arnoldi (`ARNOLDI`)—have better convergence properties but require more space. While the best method for a particular Markov chain is unclear in general, several options are available for exploration including the iterative methods described above that can be also enhanced with preconditioning, aggregation-disaggregation (`AD`), or Kronecker-specific multi-level (`ML`) methods that are inspired by multigrid and `AD` techniques. Unfortunately, we cannot acknowledge all relevant work on iterative methods due to limited space.[19,20]

A number of software tools are available that implement methods for Kronecker representations, and we selected the APNN toolbox[21] and its numerical solution package Nsolve for its rich variety of numerical techniques for the steady state analysis of Markov chains. Nsolve provides more than 70 different methods and comes with an ASCII file format for a SAN descriptor easily interfaced with our MATLAB modeling environment. Nsolve mainly supports hierarchical Markovian models that include a trivial hierarchy with a single macrostate such as Eq. 10 as a special case (see Refs. 21–24).

4. Results

In order to investigate which numerical techniques work best for the Kronecker representation of our Ca^{2+} release site models, we wrote a script for the matrix computing tool MATLAB that takes a specific Ca^{2+} release site model—defined by $K_+, K_-, \boldsymbol{e}_{\mathcal{O}}, c_\infty$, and C—and produces the input

files needed to interface with Nsolve. Using 10 three-state channels (1) we performed a preliminary study to determine which of the 70-plus numerical methods implemented in Nsolve were compatible with Eq. 10.

4.1. *Benchmark Stationary Distribution Calculations*

Table 1 lists those solvers that converged in less than 20 minutes CPU time with a maximum residual less than 10^{-12} for one configuration of 10 three-state channels. For each method we report the maximum and sum of the residuals, the CPU and wall clock times (in seconds), and the total number of iterations performed. We find that traditional relaxation methods (e.g., JOR, RSOR) work well for this problem with $3^{10} = 59,049$ states, but the addition of AD steps is not particularly helpful. AD steps do however greatly improve the performance of the GMRES solver and to a smaller extent the DQGMRES and ARNOLDI methods. The separable preconditioner (PRE) of Buchholz[23] and the BSOR preconditioner are very effective and help to reduce solution times to less than 50 seconds for several projection methods. Among ML solvers, a JOR smoother gives the best results and dynamic (DYN) or cyclic (CYC) ordering is better than a fixed (FIX) order where V, W, or F indicate the type of cycle used.[19,20]

4.2. *Problem Size and Method Performance*

In Sec. 4.1 we benchmarked the efficiency of several different algorithms that can be used to solve for the stationary distribution of Ca^{2+} release site models. To determine if this result depends strongly on problem size, we chose representatives of four classes of solvers (JOR, PRE_ARNOLDI, BSOR_BICGSTAB, and ML_JOR_F_DYN) that worked well for release sites composed of 10 three-state channels (see Table 1). Using these four methods, Fig. 2 shows the wall clock time required for convergence of $\pi^{(N)}$ as a function of the number of channels (N) for both the three- and six-state models (circles and squares, respectively). Because the N channels in each Ca^{2+} release site simulation have randomly chosen positions that may influence the time to convergence, Fig. 2 shows both the mean and standard deviation (error bars) of the wall clock time for five different release site configurations. Note that for each value of N in Fig. 2, the radius of each Ca^{2+} release site was chosen so that stochastic Ca^{2+} excitability was observed. Due to irregular release site ultrastructure, these calculations can not be simplified using spatial symmetries.

Figure 2 shows that the time until convergence is shorter when the Ca^{2+}

Table 1.   Benchmark calculations for 10 three-state channels computed using Linux PCs with dual core 3.8GHz EM64T Xeon processors and 8GB RAM solving Eq. 10.

Solver	Max Res	Sum Res	CPU	Wall	Iters
JOR	9.49E-13	5.16E-12	279	279	1840
SOR	9.49E-13	5.16E-12	435	436	1840
RSOR	8.76E-13	2.40E-12	1190	1197	990
JOR_AD	9.44E-13	5.13E-12	415	415	1550
SOR_AD	9.44E-13	5.13E-12	413	414	1550
DQGMRES	9.87E-13	6.78E-10	490	492	2940
ARNOLDI	2.42E-13	4.04E-11	214	215	1440
BICGSTAB	8.66E-13	4.89E-11	146	148	602
GMRES_AD	6.43E-13	3.61E-11	88	89	900
DQGMRES_AD	1.03E-12	1.84E-10	184	184	2008
ARNOLDI_AD	7.23E-13	7.60E-11	109	109	1280
PRE_POWER	9.37E-13	5.27E-12	246	247	1670
PRE_GMRES	8.62E-15	3.73E-12	45	46	180
PRE_ARNOLDI	8.62E-15	1.82E-12	26	27	160
PRE_BICGSTAB	4.44E-16	2.49E-14	28	28	188
BSOR_BICGSTAB	8.22E-15	5.29E-13	19	19	52
BSOR_GMRES	3.05E-13	7.73E-12	20	20	49
BSOR_TFQMR	1.83E-13	1.39E-12	17	17	48
PRE_GMRES_AD	1.29E-13	1.52E-11	36	36	140
PRE_ARNOLDI_AD	4.32E-13	7.18E-12	27	28	140
ML_JOR_V_FIX	9.69E-13	3.54E-11	105	105	372
ML_JOR_W_FIX	9.12E-13	1.14E-10	156	157	326
ML_JOR_F_FIX	9.93E-13	1.01E-10	146	146	330
ML_JOR_V_CYC	8.35E-13	6.36E-12	42	43	168
ML_JOR_W_CYC	4.36E-13	5.41E-11	26	26	38
ML_JOR_F_CYC	6.76E-13	1.39E-11	18	19	56
ML_JOR_V_DYN	8.07E-13	6.09E-12	58	59	152
ML_JOR_W_DYN	2.81E-13	5.15E-11	14	15	38
ML_JOR_F_DYN	5.87E-13	1.68E-10	15	15	46

release site is composed of three-state as opposed to six-state channels regardless of the numerical method used (compare circles to squares). Consistent with Table 1 we find that for large values of N the ML_JOR_F_DYN (black) method requires the shortest amount of time, followed by BSOR_BICGSTAB (dark gray), PRE_ARNOLDI (light gray), and finally JOR (white). Though there are important differences in the speed of the four solvers, the wall clock time until convergence is approximately proportional to the number of states (M^N), that is, the slope of each line in Fig. 2 is nearly $M = 3$ or 6 depending on the single channel model used.

We also experienced substantial differences in the amount of memory needed to run those solvers. While simple methods like JOR and SOR allocate space mainly for a few iteration vectors, Krylov subspace methods like
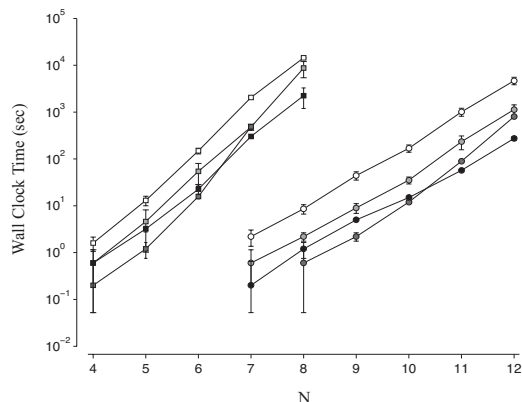
Fig. 2.   *Circles* and error bars show the mean $\pm$ SD of wall clock time for five release site configurations of the three-state model (1) using: `JOR` (*white*), `PRE_ARNOLDI` (*light gray*), `BSOR_BICGSTAB` (*dark gray*), and `ML_JOR_F_DYN` (*black*). Three-state model parameters: k_a^+ = 1.5 $\mu M^{-1} ms^{-1}$, $k_a^- = 50 ms^{-1}$, $k_b^+ = 150 \mu M^{-1} ms^{-1}$, $k_b^- = 1.5 ms^{-1}$. *Squares* and error bars give results for the six-state model (parameters as in Ref. 12). Calculations performed using 2.66 GHz Dual-Core Intel Xeon processors and 2 GB RAM.

`GMRES`, `DQGMRES` and `ARNOLDI` use more vectors (20 in the default Nsolve configuration), and this can be prohibitive for large models. For projection methods that operate on a fixed and small set of vectors like `TFQMR` and `BICGSTAB`, we observe that the space for auxiliary data structures and vectors is on the order of 7–10 iteration vectors for these models. In general we find that the iterative numerical methods that incorporate pre-conditioning techniques are quite fast compared to more traditional relaxation techniques such as `JOR`. However, the power of pre-conditioning is only evident when problem size is less than some threshold that depends upon memory limitations. On the other hand, `ML` methods are constructed to take advantage of the Kronecker representation and to have very modest memory requirements. This is consistent with our experiments that indicate `ML` methods have the greatest potential to scale well with problem size, whether that be an increase in the number of channels (N) or the number of states per channel (M).

4.3. *Comparison of Iterative Methods and Monte Carlo Simulation*

Although there may be problem size limitations, we expected that the stationary distribution of our Ca^{2+} release site models could be found more quickly using iterative methods than Monte Carlo simulation. This is confirmed in the convergence results of Fig. 3 using a release site composed of
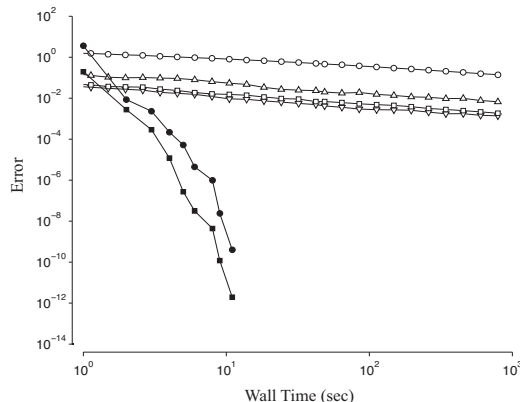
Fig. 3.   Convergence of response measures for a release site composed of 10 three-state channels using ML_JOR_F_DYN and Monte Carlo (*filled* and *open* symbols, respectively). *Circles* and *squares* give 1- and ∞-norms of the residual errors, *upper pointing triangles* give the relative error in the puff/spark *Score* for Monte Carlo (mean of 50 simulations shown) compared with the *Score* given by ML_JOR_F_DYN upon convergence. Similarly, the *lower pointing triangles* give the relative error in the probability that all N channels are closed. Parameters as in Fig. 1.

10 three-state channels for both ML_JOR_F_DYN (filled symbols) and Monte Carlo simulation (open symbols). We run a Monte Carlo simulation to estimate the stationary distribution and that estimate depends on the length of the simulation measured in seconds of wall clock time (our implementation averaged 1,260 transitions per second). The simulation starts with all N channels in state C_1—chosen because it is the most likely state at the background $[Ca^{2+}]$ (c_∞). Figure 3 shows the maximum and sum of 1- and ∞-norms of the residuals averaged over 50 simulations. As expected, the residuals associated with the Monte Carlo simulations converge much slower than those obtained with ML_JOR_F_DYN. Interestingly, Fig. 3 shows that even coarse response measures can be more quickly obtained using numerical iterative methods than Monte Carlo simulation. We find that the relative errors of the puff/spark *Score* (upwards pointing triangles) and the probability that all N channels were closed (downwards pointing triangles) obtained via Monte Carlo simulation did not converge significantly faster than the maximum residual error (open squares).

5. Conclusions

We have presented a Kronecker structured representation for Ca^{2+} release sites composed of Ca^{2+}-regulated Ca^{2+} channels under the assumption that these channels interact instantaneously via the buffered diffusion of intra-

cellular Ca^{2+} (Sec. 2). Because informative response measures such as the puff/spark *Score* can be determined if the steady-state probability of each release site configuration is known, we have identified numerical interative solution techniques that perform well in this biophysical context.

The benchmark stationary distribution calculations presented here indicate significant performance differences among iterative solution methods. Multi-level methods provide excellent convergence with modest additional memory requirements for the Kronecker representation of our Ca^{2+} release site models. When the available main memory permits, `BSOR`-preconditioned projection methods such as `TFQMR` and `BICGSTAB` are also effective, as is the method of Arnoldi combined with a simple preconditioner. In case of tight memory constraints, Jacobi and Gauss-Seidel iterations are also possible (but slower). When numerical iterative methods apply, they outperform our implementation of Monte Carlo simulation for estimates of response measures such as the puff/spark *Score* and the probability of a number of channels being in a particular state.

Single channel models of IP$_3$Rs and RyRs can be significantly more complicated than the three- and six-state models that are the focus of this manuscript. For example, the well-known DeYoung-Keizer IP$_3$R model includes four eight-state subunits per channel for a total of 330 distinguishable states.[25] Because biophysically realistic Ca^{2+} release site simulations can involve tens or even hundreds of intracellular channels, we expect that the development of approximate methods for our SAN descriptor (Eq. 10) will be an important aspect of future work. Of course, some puff and spark statistics—such as puff/spark duration and inter-event interval distributions—cannot be determined from the Ca^{2+} release site stationary distribution. Consequently, it will be important to determine if transient analysis can also be accelerated by leveraging the Kronecker structure of Ca^{2+} release sites composed of instantenteously coupled Ca^{2+}-regulated Ca^{2+} channels. Furthermore, although the SAN conceptual framework and its associated analysis techniques presented in this manuscript have focused solely on the emergent dynamics of Ca^{2+} release sites, it is also important to note that these techniques should be generally applicable to our understanding of signaling complexes of other kinds.[26,27]

Acknowledgments

References

1. D. Colquhoun and A. Hawkes, A Q-matrix cookbook: how to write only one program to calculate the sigle-channel and macroscopic predictions for any kinetic mechanism, in *Single-Channel Recording*, eds. B. Sakmann and E. Neher (Plenum Press, New York, 1995) pp. 589–633.
2. G. Smith, Modeling the stochastic gating of ion channels, in *Computational Cell Biology*, eds. C. Fall, E. Marland, J. Wagner and J. Tyson (Springer-Verlag, 2002) pp. 291–325.
3. F. Ball, R. Milne, I. Tame and G. Yeo, *Advances in App Prob* **29**, 56 (1997).
4. F. Ball and G. Yeo, *Methodology and Computing in App Prob* **2**, 93 (1999).
5. H. Cheng, W. Lederer and M. Cannell, *Science* **262**, 740 (1993).
6. H. Cheng, M. Lederer, W. Lederer and M. Cannell, *Am J Physiol* **270**, C148 (1996).
7. Y. Yao, J. Choi and I. Parker, *J Physiol* **482**, 533 (1995).
8. I. Parker, J. Choi and Y. Yao, *Cell Calcium* **20**, 105 (1996).
9. M. Berridge, *J Physiol (London)* **499**, 291 (1997).
10. V. Nguyen, R. Mathias and G. Smith, *Bull. Math. Biol.* **67**, 393 (2005).
11. S. Swillens, G. Dupont, L. Combettes and P. Champeil, *Proc Natl Acad Sci USA* **96**, 13750(Nov 1999).
12. H. DeRemigio, P. Kemper, M. LaMar and G. Smith, *Technical Report* **WM-CS-2007-06** (2007).
13. G. Smith, An extended DeYoung-Keizer-like IP$_3$ receptor model that accounts for domain Ca^{2+}-mediated inactivation, in *Recent Research Developments in Biophysical Chemistry, Vol. II*, eds. C. Condat and A. Baruzzi (Research Signpost, 2002).
14. I. Bezprozvanny, *Cell Calcium* **16**, 151 (1994).
15. M. Naraghi and E. Neher, *J Neurosci* **17**, p. 6961(6973 1997).
16. G. Smith, L. Dai, R. Muira and A. Sherman, *SIAM J Appl Math* **61**, 1816 (2001).
17. W. Stewart, *Introduction to the Numerical Solution of Markov Chains* (Princeton University Press, Princeton, 1994).
18. D. Gillespie, *J Comp Phys* **22**, 403 (1976).
19. P. Buchholz and T. Dayar, *Computing* **73**, 349 (2004).
20. P. Buchholz and T. Dayar, *SIAM Matrix Analysis and App (to appear)* (2007).
21. P. Buchholz and P. Kemper, A toolbox for the analysis of discrete event dynamic systems., in *CAV. LNCS 1633*, 1999.
22. P. Buchholz and T. Dayar, *SIAM J. Sci. Comput.* **26**, 1289 (2005).
23. P. Buchholz, Projection methods for the analysis of stochastic automata networks, in *Numerical Solution of Markov Chains*, eds. B. Plateau, W. Stewart and M. Silva (Prensas Univerversitarias de Zaragoza, 1999) pp. 149–168.
24. P. Buchholz, *Prob in the Eng and Informational Sci* **11**, 229 (1997).
25. G. De Young and J. Keizer, *Proc Natl Acad Sci USA* **89**, 9895 (1992).
26. J. Schlessinger, *Cell* **103**, 211 (2000).
27. H. Husi, M. A. Ward, J. S. Choudhary, W. P. Blackstock and S. G. Grant, *Nat Neurosci* **3**, 661 (2000).